Investigation of structure and dynamics of the hydrated metal–organic framework MIL-53(Cr) using first-principles molecular dynamics

Volker Haigis, François-Xavier Coudert, Rodolphe Vuilleumier, Anne Boutin

Investigation of structure and dynamics of the hydrated metal-organic framework MIL-53(Cr) using first-principles molecular dynamics

Volker Haigis,*[a] François-Xavier Coudert,[b] Rodolphe Vuilleumier[a] and Anne Boutin[a]

The hydration behavior of metal-organic frameworks (MOFs) is of interest both from a practical and from a fundamental point of view: it is linked, on the one hand, to the hydrothermal stability (or instability) of the nanoporous material, which might limit its use in technological applications. On the other hand, it sheds light on the behavior of water in a strongly confined environment. Here, we use first-principles molecular dynamics (MD) to investigate two hydrated phases of the flexible MOF MIL-53(Cr), which adopts a narrow- or a large-pore form, depending on the water loading. Structure and dynamics of the two phases are thoroughly analyzed and compared, with a focus on the hydroxyl group of MIL-53(Cr) and the water molecules in the nanopores. Furthermore, the behavior of the confined water is compared to that of bulk water. Whereas in the narrow-pore form, water is adsorbed at specific crystalline sites, it shows a more disordered, bulk-like structure in the large-pore form. However, reorientation dynamics of water molecules in the latter is considerably slowed down with respect to bulk water, which highlights the confinement effect of the nanoporous framework.

1 Introduction

Metal–organic frameworks (MOFs) are a topical class of nanoporous materials displaying a large range of crystal structures and host–guest properties, due to a combination of tunable porosity, by choice of metal centres and linker length, and functionalisation of the internal surface of the material. They have gained a lot of attention in the last decade and have been proposed for use in applications such as adsorptive storage, gas separation, catalysis and sensing. However, even though a rapidly increasing number of structures have been synthesized, there are far less detailed characterizations of water adsorption in MOFs in the literature [1–9] than adsorption studies on other gases of strategic interest, such as carbon dioxide, methane and hydrogen. Nonetheless, the behavior of MOFs in presence of water vapor, their stability under humidity and the impact of water adsorption on their other physical and chemical properties (adsorptive separation performance, catalysis, etc.) are of primary importance if one envisions applications at the industrial level.

Our interest in the present work is to characterize the structure, vibrational and orientational dynamics of water confined in the archetypical material MIL-53(Cr). This material is formed of unidimensional chains of corner-sharing $CrO_4(\mu_2\text{-}OH)_2$ octahedra, linked by 1,4-benzenedicarboxylate (BDC) ligands to form linear diamond-shaped channels large enough to accommodate small guest molecules [10] (Fig. 1). This structure may oscillate between two phases: a large-pore (lp) structure and a narrow-pore (np) one. This phenomenon, which has been termed "breathing", can be induced by adsorption or desorption of guest molecules including water [11,12], variations in temperature [13] or mechanical stress [14]. Full studies of adsorption and desorption of water, among other polar vapors, in MIL-53(Cr) were published by Bourrelly *et al.* [15] and Devautour-Vinot *et al.* [16] including experimental sorption characterization, calorimetric measurements and quantum chemistry calculations of the preferential arrangements of the molecules within the pores. These quantum chemistry calculations, performed at the density functional theory [17,18] (DFT) level, were geometry optimizations leading to water structures of lowest energy for each phase of the host (narrow and large pore). A later experimental study of MIL-53(Cr) immersed in liquid water used high resolution powder X-ray diffraction to solve the structure of the pores of both the large-pore and narrow-pore phases, fully filled with water [19].

In addition, recent molecular simulation studies have used force field-based molecular dynamics and grand canonical Monte-Carlo simulations to study the structure, diffusion and adsorption thermodynamics of water in the lp and np phases of MIL-53(Cr) [20,21]. The two works differ in their specifics: Salles *et al.* [20] focused on classical (Newtonian) dynamics of the water and framework, while Paesani [21] used normal-mode path integral molecular dynamics in order to include quan-

[a] *CNRS-ENS-UPMC, Département de Chimie, École Normale Supérieure, 24 rue Lhomond, 75005 Paris, France. Tel.: +33 1 44 32 33 38; E-mail: volker.haigis@ens.fr*

[b] *CNRS & Chimie ParisTech, 11 rue Pierre et Marie Curie, 75005 Paris, France.*

tum dynamical effects. However, both studies described the interactions in the system at the classical level, with the use of a parameterized nonpolarizable force field. Furthermore, Salles *et al.* [20] describe the water molecule as a rigid body. Both approximation are quite drastic, and may limit the precision with which water–MOF and water–water interactions are described. Indeed, a recent report by Cirera *et al.* [22] demonstrated that the effects of electronic polarization significantly impact the structure of water in the pores of MIL-53(Cr), especially at large loading of the unit cell (fully hydrated pores). Very recently, Chen *et al.* [23] published an ab-initio study on the structural response of the Sc-bearing MIL-53(Sc) to temperature changes and CO_2 adsorption.

Here, we present a study of the structure and dynamics of the fully hydrated MIL-53(Cr) np and lp phases, using first-principles molecular dynamics. We used Car–Parrinello molecular dynamics, meaning that the interactions in the system are treated at the quantum mechanical level, in the DFT approach, while the molecular dynamics samples the phase space of the system and allows the calculation of statistical averages and dynamical properties (and not only minimal energy configurations, as in quantum chemistry energy minimizations). We have shown earlier that this approach allows a good description of the structure, dynamics, electronic properties and reactivity of molecular fluids confined in porous spaces. In particular, we showed how it could describe the behavior of water confined in a family of zeolites[24,25] and explain the limited hydrothermal stability of MOFs from the IR-MOF family[9]. Compared to simulations based on empirical force fields, the first-principles molecular dynamics approach has the advantage that it does not depend on empirical parameters and hence is transferable to very different chemical environments, e.g. situations where chemical reactions occur. Moreover, in the present case of nano-confined water, the validity of classical force fields has to be checked carefully since they are parameterized for bulk water in general and might not perform well in surface-dominated systems. With the first-principles approach, we aim at providing a reliable reference and at validating previous results obtained from force-field simulations. Also, it paves the way for future studies of chemical reactivity in these systems. However, the high computational costs of this approach impose limits on the system size and simulation times, and phenomena such as gas diffusion in nanoporous materials may still lie beyond the capabilities of first-principles simulations.

2 Computational methods

The hydrated phases of MIL-53(Cr) were studied by means of DFT-based Car-Parrinello molecular dynamics simulations as implemented in the CPMD package[26,27]. The simulation cell represents one unit cell of the empty (non-hydrated) MIL-53(Cr), containing 4 [Cr(OH)-(O_2C-C_6H_4-CO_2)], and the hydrated narrow- and large-pore phases were modeled by adding 4 and 24 water molecules, respectively, to the empty framework. This corresponds to the amount of water found experimentally in the two phases[19]. The simulations were performed in the canonical ($NV\,T$) ensemble, with experimental unit cell parameters taken from Guillou *et al.* [19] . The temperature of the ions was maintained at 350 K by a Berendsen thermostat with a coupling time constant of 0.5 ps. It was shown that time constants larger than 0.1 ps yield reliable structural and dynamical properties of water[28]. Another Berendsen thermostat was used to constrain the kinetic energy of the fictitious degrees of freedom with a coupling time constant of 0.25 ps. The mass associated with the latter was chosen to be 200 a.u., and a time step of 0.05 fs was used for the integration of the equations of motion. The interactions between electrons and ion cores were described by Troullier-Martins pseudopoten-tials[29], and the PBE exchange-correlation functional[30] was used. Dispersion interactions, which are known to be poorly represented by the semilocal PBE functional, were included via the scheme proposed by Grimme [31] . A plane-wave cut-off of 120 Ry was found to be sufficient to obtain converged ionic forces. All simulations were started from the structures of hydrated MIL-53(Cr) as determined by x-ray diffraction (narrow-pore and large-pore form, Guillou *et al.* [19]). Since the hydrogen atoms are not visible by x-ray diffraction, we added them "by hand" in reasonable positions. For compu-tational convenience, the heavier deuterium isotope was used throughout the study. Its larger mass slows down the hydrogen dynamics and allows using a larger time step, without affect-ing the chemical properties of the system. The limited size of the simulation cell is due to the high computational demands of first-principles simulations and might affect properties such as the kinetics of phase transitions or diffusion coefficients, and these phenomena are therefore not discussed in this study. However, the finite-size effect on structural, vibrational, and rotational properties is expected to be small.

In addition to the simulations of MIL-53(Cr), we generated a trajectory of 13 ps for bulk water, represented by 64 H_2O molecules in a periodically repeated simulation cell and with a density of 1 g/cm^3. The settings for this simulation was the same as for MIL-53(Cr), except for a larger mass of 400 a.u. of the fictitious degrees of freedom, which were not thermostat-ted, and a larger time step of 0.073 fs.

3 Results and discussion

3.1 Structure of the narrow-pore and large-pore phases

The hydrated narrow-pore phase with four water molecules in the simulation box, named MIL-53(Cr)(1H_2O per Cr), was equilibrated for 5 ps and subsequently simulated for another

30 ps. During the whole simulation, the oxygen atoms of the water molecules formed hydrogen bonds with the hy-droxyl groups of the MIL-53 framework. No hopping of water molecules to neighboring binding sites was observed within the time span of the MD run. This suggests that the wa-ter inside the narrow pores may be considered as part of the crystal structure rather than a fluid phase. To corroborate this finding, we averaged, over the whole trajectory, the positions of all atoms, except the hydrogen atoms belonging to water molecules, and checked the resulting structure for symmetry. It was found that the average structure has indeed space group $C2/c$, the same as the non-hydrated MIL-53(Cr). The wa-ter hydrogen atoms were excluded from this analysis because they rotate freely about the dipole axis of the water molecules, and hence their average positions are not meaningful. The av-erage structure is shown in Fig. 1.

The simulation of the hydrated large-pore phase with 24 wa-ter molecules in the simulation box, named MIL-53(Cr) ($6H_2O$ per Cr), was started from the structure determined by x-ray diffraction[19]. The system was equilibrated for 5 ps and sub-sequently simulated for another 25 ps. For the Rietveld re-finement of the X-ray data, the authors imposed symmetry constraints on the positions of the water molecules. How-ever, in our simulations, no symmetry was assumed, and all atoms were completely free to move within the orthorhombic simulation box. This enabled us to check whether the water molecules within the pores really occupy well-defined crys-talline sites or if they form a more disordered structure, pos-sibly resembling bulk water. Indeed, a disordered hydration structure was found in this case, which will be disussed in sec-tion 3.4.1. Regarding the average structure of the framework itself, a tilting of the organic ligands with respect to the plane defined by neighboring inorganic chains is observed, which was not seen in the x-ray diffraction. Because this tilting is one of two symmetrically equivalent tilts, it is thus absent from the experimental crystallographic structure, which is an aver-age (non-tilted) structure of the two conformations.

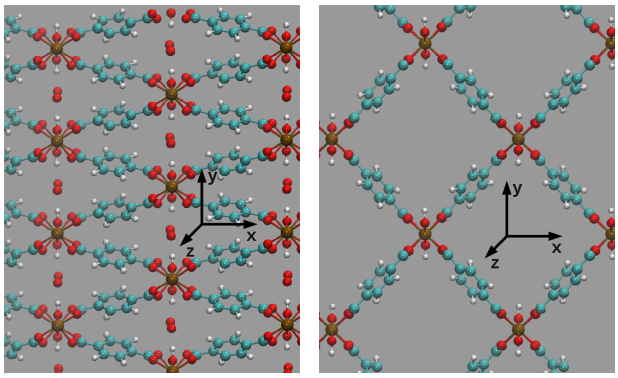

Fig. 1 Left: Structure of the hydrated narrow-pore phase, averaged over the trajectory. For clarity, the H atoms of the water molecules are not shown. Right: Structure of the hydrated large-pore phase, averaged over the trajectory. For clarity, the water molecules are not shown. Color code: Cr—brown, O—red, C—blue, H—white.

3.2 Behavior of hydroxyl groups

We then turned our attention to the dynamics of the hydroxyl group of the Cr(μ_2-OH) inorganic chain of the MIL-53(Cr) framework. While its oxygen atom is rather constrained and has a low amplitude of movement, with an average mean square displacement of about 0.2 Å with respect to its average position (see Table 1), the position of the hydrogen atom (and thus the orientation of the μ_2-OH group) vary more widely during the course of our simulations. In both the lp and np phases, the average position of the H atom lies in the CrOCr plane, but exhibits large wagging motions around this sym-metric position. We quantified these by plotting the distribu-tions of the angles between the μ_2-OH group and the CrOCr plane during the molecular dynamics (Fig. 2). It can be seen that in both structures, the wagging motion of the μ_2-OH group can reach angles of up to 40°, with a slightly larger am-plitude for the narrow-pore phase than in the large-pore phase (respective full half width of the distribution: 33°and 27°; ob-tained from a Gaussian fit). We attribute this difference to larger steric hindrance in the lp phase, due to the high den-sity of water molecules inside the porous channels. A similar conclusion can be reached on the basis of the mean square dis-placement of the H atom from its mean position, with values of 0.314 Å and 0.305 Å in the np and lp phases. This large amplitude of the wagging motion is consistent with the fact that the proton position could not be solved in the experimen-tal crystallographic structures. Remarkably, the Gaussian-like nature of the μ_2-OH wagging angle reveals that this vibration mode is harmonic in nature, even with such a large amplitude.

species	np phase	lp phase
$O_{\mu_2\text{-OH}}$	0.200 Å	0.207 Å
$H_{\mu_2\text{-OH}}$	0.314 Å	0.305 Å
O_w	0.811 Å	0.484 Å

Table 1 Mean square displacement for selected species with respect to their average position, averaged over equivalent atoms. For the lp phase, only the hydroxyl groups and the water molecules which remain hydrogen-bonded to each other during the whole simulation are taken into account.

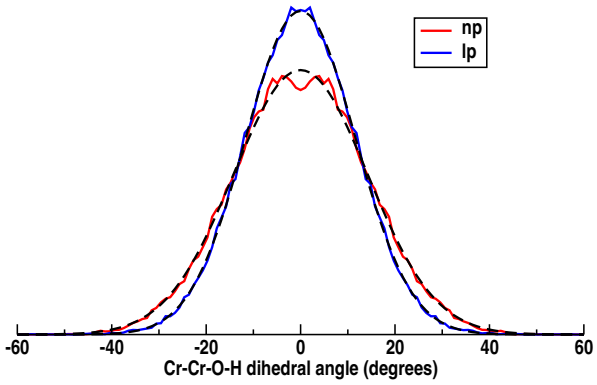

Fig. 2 Distribution of the angle between the μ_2-OH group of the inorganic chain and the CrOCr plane, in the hydrated large-pore (lp) and narrow-pore (np) phases of MIL-53(Cr). Dashed lines represent Gaussian fits.

3.3 Water molecules bound to μ_2-OH groups

After characterizing the μ_2-OH group of the MIL-53(Cr) material, we now focus on the water molecules hydrogen-bonded to these groups. As discussed in section 3.1, the situation here is very different between the narrow-pore and large-pore phases. In the np phase, there is a 1:1 stoichiometry between water and μ_2-OH, with each water molecule bound to an hydroxyl group, with O—O distances and O—H—O angles typical of hydrogen bonds. No hopping of the water was observed during the 30 ps of dynamics. However, while the water molecules do not diffuse, they show large orientational freedom: the molecules rotate rather freely in a half-space, while keeping intact the hydroxyl–water hydrogen bond. As a part of this rotational diffusion, we observe during the dynamics many instances where a water's H atom comes in close vicinity of a neighboring carboxylate group. In the closest case, we observed O_{water}–$O_{carboxylate}$ distances down to 2.5 Å, and H_{water}–$O_{carboxylate}$ distances down to 1.6 Å. However, such events cannot be construed as proper hydrogen bonds on account of their short lifetime (typically less than 200 fs). A similar phenomenon is known to take place for water confined in siliceous zeolites, and is not due to specific water–material interactions but merely to the narrow confinement of the water molecule[25].

In the large-pore phase, the situation is quite different. Out of the four μ_2-OH groups in the unit cell, three remain hydrogen-bonded to the same three water molecules throughout the molecular simulation. For the fourth hydroxyl, however, we do observe an exchange of the hydrogen-bonded water molecule twice during the dynamics. This can be seen in Fig. 3 (upper panel), where we plot the $O_{\mu_2\text{-OH}}$–O_{water} distance of three water molecules near this fourth μ_2-OH. The exchange of water molecules bonded to the μ_2-OH group can be

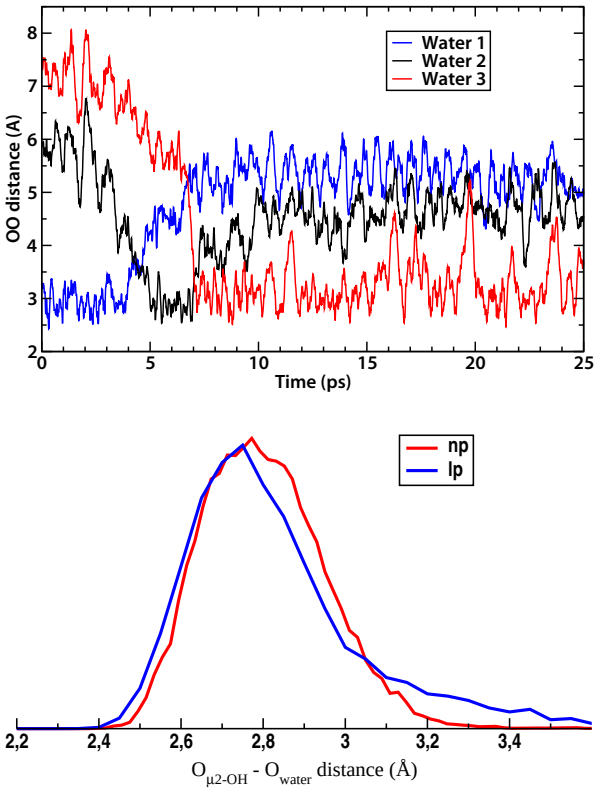

Fig. 3 Upper panel: time evolution of the $O_{\mu_2\text{-OH}}$–O_{water} distance of three water molecules near an μ_2-OH group (see text for details). Lower panel: distribution of $O_{\mu_2\text{-OH}}$–O_{water} in the hydrated np and lp phases.

seen at $t = 4$ ps and 7 ps. Even after 7 ps, the plot still reveals some large fluctuations of the O–O distance, with peaks up to 5 Å. This weaker hydrogen bonding is also reflected in the histogram of $O_{\mu_2\text{-OH}}$–O_{water} distances (Fig. 3, lower panel), which shows a long tail at large distances for the lp phase, in contrast with the narrow-pore case.

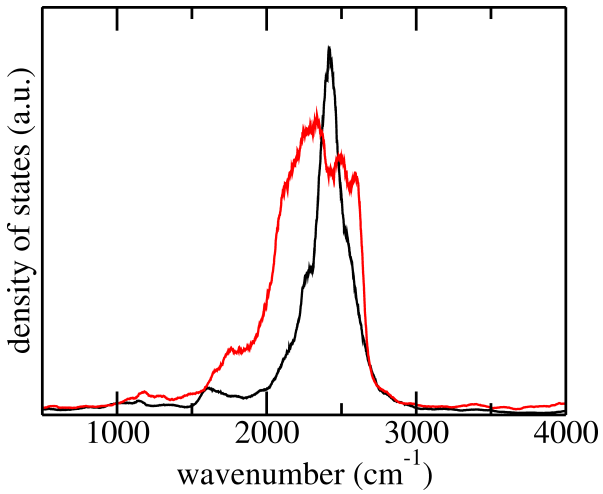

Fig. 4 Spectrum of the μ_2-OH stretching vibration in the narrow-pore (black) and the large-pore (red) phase, obtained from Fourier-transforming the velocity autocorrelation function of the μ_2-OH vibrations.

This distribution of $O_{\mu_2\text{-OH}}$–O_{water} distances can be related to the vibrational spectrum of the μ_2-OH group, which was obtained from the MD trajectories by Fourier-transforming the velocity autocorrelation function of μ_2-OH bond vibrations (Fig. 4). The spectra of the narrow- and the large-pore form both represent an average over all four hydroxyl groups in the simulation cell. Since in the simulations, hy-drogen was represented by deuterium isotopes, the wavenum-bers of μ_2-OH vibrations lie below the usual values around 3400 cm^{-1}. While the narrow-pore phase exhibits a well-defined peak around 2400 cm^{-1}, the spectrum of the large-pore phase is considerably broadened. This finding is in line with the more disordered hydration structure found in the lat-ter (see section 3.4.1) and is a direct consequence of the wider distribution of $O_{\mu_2\text{-OH}}$–O_{water} distances in the large-pore phase (Fig. 3). The weaker hydrogen bonding resulting from the pro-nounced tail of the $O_{\mu_2\text{-OH}}$–O_{water} distances leads to a large-wavenumber shoulder in the μ_2-OH stretching vibrations be-tween 2500 cm $^{-1}$ and 2700 cm^{-1}, which is not observed in the narrow-pore phase.

At this point, we would like to comment on a point discussed by Cirera *et al.* [22] who used classical force fields to investigate the hydrogen bonding between water molecules and the μ_2-OH groups in hydrated MIL-53(Cr). They found

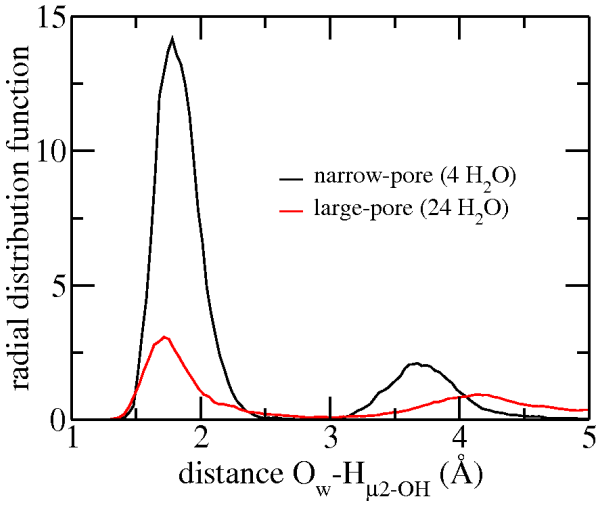

Fig. 5 Radial distribtion functions for O_{water}–$H_{\mu_2\text{-OH}}$ in the narrow-pore (black) and large-pore (red) phase.

that a polarizable force field leads to a substantially different structure than a non-polarizable model. In particular, with a polarizable force filed, Cirera *et al.* [22] obtained a pronounced peak in the radial distribution function for water oxygen atoms and the H atoms of μ_2-OH groups just below 2 Å (Fig. 4 in their study). This peak was weakened – and even absent at high water loadings – when the non-polarizable force field was used. The authors concluded that polarizability is essential in order to capture correctly the water–framework interaction. Our DFT simulations provide a suitable reference to check this statement, since the electronic degress of free-dom are treated explicitly and hence polarizability is automat-ically taken into account. Fig. 5 shows the radial distribu-tion function for $O_{\mu_2\text{-OH}}$–O_{water} in the narrow- and large-pore phase. Indeed, we obatained a strong peak around 1.8 Å in both cases, confirming the importance of polarizability to describe water–framework interactions accurately. However, we also found significant differences between the first-principles and the force-field simulations: at high water loading of MIL-53(Cr), the radial ditribution function goes to zero at distances around 3 Å (Fig. 5) in our simulations, whereas it is almost flat above 2.5 Å with the polarizable force field of Cirera *et al.* [22].

Finally, we look at the environment of the μ_2-OH-bound water molecules in the large-pore phase, and their hydrogen bonding pattern to neighboring molecules. Like in the case of the np phase, they can get close to the carboxylate groups of the framework, without forming H bonds. However, because of the presence of more water molecules in the larger pores, they do form H bonds with other water molecules. These hydrogen bond networks are naturally dynamic and live for few picoseconds, but two specific arrangements are repeatedly observed: a 2A1D (“A”: accepting, “D”: donating) configura-

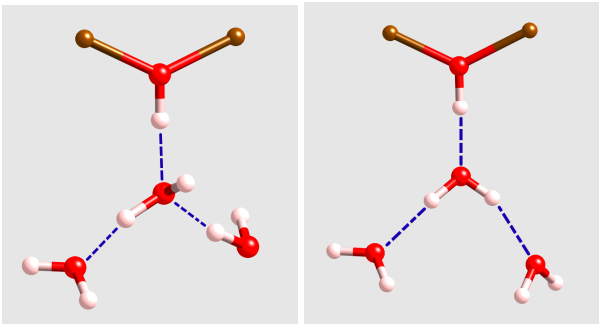

Fig. 6 Snapshots of typical hydrogen bond arrangements of the μ_2-OH-bound water molecule in MIL-53(Cr) lp phase.

tion, in which the μ_2-OH-bound water molecule is H-bond donor to one other molecule, and H-bond acceptor for the μ_2-OH group and one H_2O; a 1A2D, where the μ_2-OH-bound water molecule is H-bond donor for two neighboring water molecules. Snapshots of these typical arrangements are depicted in Fig. 6. This is to be contrasted with the typical "2A2D" configuration in bulk water, where a water molecule accepts two and donates two H bonds.

3.4 "Bulk-like" water in the large-pore phase

3.4.1 Structure Fig. 7 shows the radial distribution functions for oxygen atoms which are part of water molecules (O_{water}, upper panel) and for O_{water}-H pairs (lower panel). For comparison, bulk water is also shown. The broad peaks indicate a liquid-like structure. The first and second peak in the O_{water}-O_{water} distribution are located at 2.8 Å and 4.5 Å, respectively, in fair agreement with experimental data on bulk water at ambient conditions[32] as well as with the bulk water simulation results. Regarding the radial distribution of O_{water}-H pairs, three peaks were found in the simulation: the first one at 1 Å corresponds to intramolecular bonding, the second one around 1.8 Å falls into the range of typical hydrogen bond lengths, and the third peak at 3.3 Å comprises non-bonded O_{water}-H pairs. Note that for this analysis, all hydrogen atoms were taken into account, including those which are part of the MIL-53 framework. While the overall shape of the distribution functions resembles that of bulk water, the water inside the framework exhibits higher peaks and therefore appears to be more strongly structured.

While radial distribution functions reveal important aspects of liquid structure, they represent an isotropic average and are not unique, in the sense that very different atomic structures can lead to the same radial distribution functions. Additional information is contained in the distribution of angles formed by triplets of atoms. Fig. 8 shows the distribution of angles defined by three neighboring O_{water}, and for reference, the bulk water distribution is plotted. The distribution forms a broad

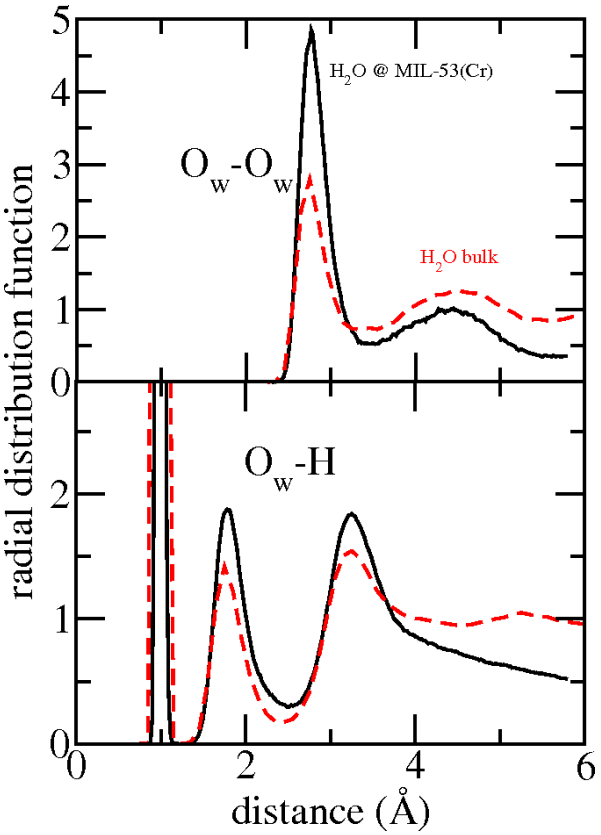

Fig. 7 Radial distribution functions of water inside the MIL-53(Cr) large-pore phase (black). Upper panel: pair distribution of water oxygen (O_{water}), lower panel: pair distribution of O_{water} and H. Red dashed line: bulk water.

peak around 105°, close to the tetrahedral angle of 109.5°, with a minor feature at 50°. The distance cutoff for neighboring O_{water} was set to 3.5 Å, which corresponds to the first minimum of the respective radial distribution function, see Fig. 7. The angle distribution indicates that the O_{water} form a network of more or less distorted tetrahedra, as expected for bulk water and also seen in the bulk water simulations. However, water in the MIL-53(Cr) framework shows a narrower distribution than bulk water, which corroborates the slightly overstructured nature of the confined liquid. The peak at small angles (in both the bulk and the confined water phase) results from a combined excluded-volume and entropy effect: O^1_w–O^2_w–O^3_w angles smaller than 45°generate too short O^1_w–O^3_w distances. On the other hand, small angles are entropically favorable because they increase the available configuration space for other neighboring O_{water}. In a compromise, water configurations accumulate around the smallest possible angle, which leads to the peak at 50°.

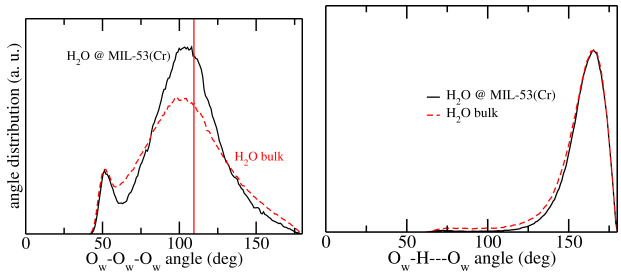

Fig. 8 Left: Angle distribution for O_{water} triplets in MIL-53(Cr), large-pore phase (black line). The red vertical line defines the tetrahedral angle of 109.5°. The dashed red line represents bulk water. Right: Angle distribution for O_{water}-H—O_{water} triplets in MIL-53(Cr), large-pore phase (black line).

In Fig. 8, we also plot the distribution of the angles between the intramolecular O_{water}-H bond and the hydrogen bond formed by the same H. A cutoff of 1.25 Å and 2.5 Å was used for intramolecular and hydrogen bonds, respectively, as determined from the minima of the radial distribution functions, see Fig. 7. A broad peak is found which exhibits a maximum at 165°. The distributions of confined and bulk water are of very similar shape.

3.4.2 Water reorientation dynamics Given the structural similarities of water confined in the large-pore phase and bulk water, one might prematurely conclude that the behavior of the confined water is already close to the bulk limit. However, this limit is characterized not only by structure but also by dynamical properties. We therefore investigated the reorientation dynamics of water inside the MIL-53(Cr) framework by means of the correlation function

$$C(t) = \langle \mathbf{u}(0) \cdot \mathbf{u}(t) \rangle \qquad (1)$$

where $\mathbf{u}(t)$ is the normalized bisector of the H-O-H angle of a water molecule at time t, and the average $\langle \ldots \rangle$ is taken over all water molecules and different time origins. In order to obtain information on possible anisotropic dynamics, we also calculated the component-wise correlation functions

$$C_\alpha(t) = \langle u_\alpha(0) u_\alpha(t) \rangle \qquad (2)$$

with $\alpha \in \{x, y, z\}$. They sum up to the total $C(t)$ at every instant of time.

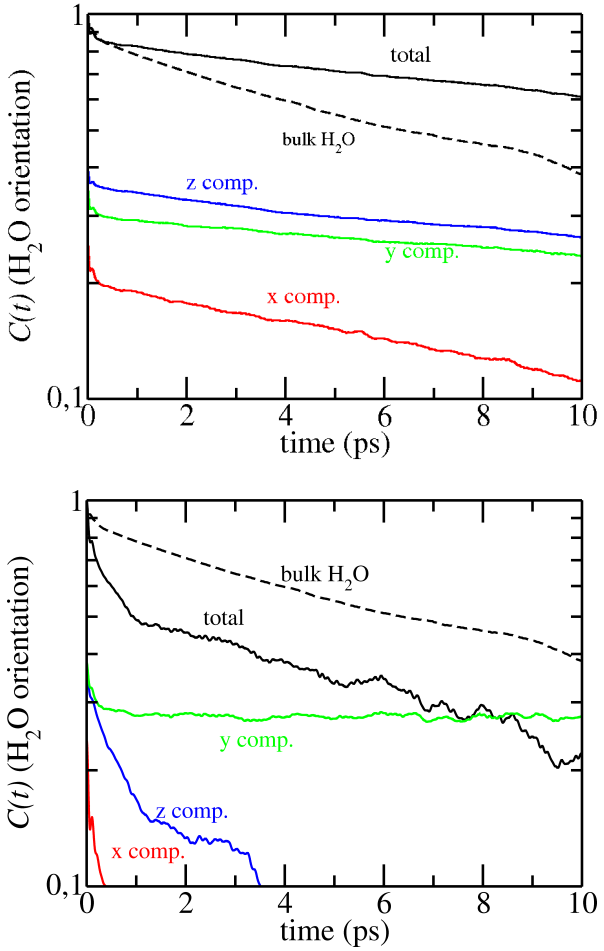

Fig. 9 Reorientation dynamics of water in the large-pore (upper panel) and narrow-pore (lower pannel) phase, characterized by the total correlation function $C(t)$ (black line). The bulk water reference is shown as a dashed line. The colored curves represent component-wise correlation functions (eq. 2).

The results for the large- and narrow-pore phases are shown in Fig. 9. In the large-pore phase, the total correlation functions decays much more slowly than in bulk water (dashed line). For the time interval 1 ps $< t <$ 10 ps, it can be fitted by an exponential $C(t) = A\exp(-t/\tau)$ with a time constant

$\tau = 32$ ps. For bulk water, a value of $\tau = 13$ ps is obtained, i.e. we find a ratio $\tau_{lp}/\tau_{bulk} = 2.5$. The component-wise correlation functions reveal anisotropic behavior: the values of $C_\alpha(t=0)$ indicate a preferential orientation of the H-O-H bisector along z and y, i.e. along the diamond-shaped channels of the framework and in the direction joining opposite μ_2-OH groups (see Fig. 1 for the labelling of the axes). Furthermore, the z and y components decay more slowly than the x component and are thus responsable for the retarded decay of the total correlation function with respect to the one of bulk water. We note that at the time scale of several nanoseconds, which is not accessible by DFT-based MD, Salles *et al.* [20] found relaxation times up to 2 ns, using an empirical force field and water loadings different from ours.

In the narrow-pore phase, on the other hand, $C(t)$ decays very rapidly for short times $t < 1$ ps. At larger times, the highly anisotropic nature of the reorientation dynamics prevents us from reducing it to a single time constant by an exponential fit. The component-wise correlation functions reveal that again, the water orientation along y and z is strongly preferred. While C_x and C_z decrease rapidly, C_y remains constant after an initial decay. This reflects the stability of the water ori-entation, pointing away from the μ_2-OH groups of the frame-work, and we anticipate that the constant C_y will eventually dominate the total $C(t)$ at large t. Hence a significantly slower relaxation is expected for large time scales.

In our approach, the atomic nuclei follow a classical trajectory on a potential energy surface determined by quantum interactions. In general, the quantum nature of the nuclei, in particular of the protons in water molecules, can strongly affect the dynamical properties of a system. However, in the present case, the effect of quantum dynamics seems to be largely reduced by the confinement of water in nanopores: Paesani [21] found that relaxation times for the reorientation of water molecules in MIL-53(Cr), derived from classical and quantum dynamics, agree to within a factor 1.3 for most water loadings, and always to within a factor of 1.6. A direct comparison of our relaxation times to their results is problematic since they used a slightly different definition of the orientation correlation function. However, it is interesting to note that in the large-pore phase, the ratio $\tau_{lp}/\tau_{bulk} = 2.4$ found by Paesani [21] using classical MD agrees remarkably well with our value of 2.5.

4 Conclusions

The present work demonstrates that first-principles molecular dynamics simulations are a useful and computationally affordable tool for investigating structural and vibrational properties of metal-organic frameworks, providing information which is not easily accessible by experimental techniques. Our simulations revealed a markedly different hydration behavior of the narrow- and large-pore phases of MIL-53(Cr): In the narrow-pore form of the material, water occupies proper crystalline sites, although with large vibrations around the equilibrium position. The large-pore phase, on the other hand, exhibits a more disordered hydration in which the adsorbed water shows a structure similar to that of bulk water, although with slightly different H bond arrangements. Regarding the dynamics of water in MIL-53(Cr), the mean square displacement of water molecules bound to μ_2-OH groups in the framework is considerably larger in the narrow- than in the large-pore structure. This can be understood in terms of the steric hindrance due to other water molecules in the strongly hydrated large-pore phase, which is absent in the narrow-pore case. Similarly, water reorientation dynamics are distinctly slower in the large- than in the narrow-pore phase. Moreover, reorientation of water molecules in the large-pore form is almost three times slower than in bulk water. This indicates that water in the pores of MIL-53(Cr), although structurally similar to bulk water, displays very clearly the impact of the confinement on its dynamics.

5 Acknowledgments

The authors acknowledge funding from the Agence Nationale de la Recherche under the project "SOFT-CRYSTAB" (ANR-2010-BLAN-0822) and generous allocation of computing time by GENCI (grant i2013087069).

References

1 J. A. Greathouse and M. D. Allendorf, *J. Am. Chem. Soc.*, 2006, **128**, 10678–10679.
2 A. Kondo, T. Daimaru, H. Noguchi, T. Ohba, K. Kaneko and H. Kanoh, *J. Colloid. Interface Sci.*, 2007, **314**, 422–426.
3 Y. Li and R. T. Yang, *Langmuir*, 2007, **23**, 12937–12944.
4 J. Y. Lee, D. H. Olson, L. Pan, T. J. Emge and J. Li, *Adv. Funct. Mater.*, 2007, **17**, 1255–1262.
5 J. M. Castillo, T. J. H. Vlugt and S. Calero, *J. Phys. Chem. C*, 2008, **112**, 15934–15939.
6 A. O. Yazadin, A. I. Benin, D. A. Faheem, P. Jakubczak, J. J. Low, R. R. Willis and R. Q. Snurr, *Chem. Mater.*, 2009, **21**, 1425–1430.
7 P. Küsgens, M. Rose, I. Senkovska, H. Fröde, A. Henschel, S. Siegle and S. Kaskel, *Micoporous Mesporous Mater.*, 2009, **120**, 1325–330.
8 S. Paranthaman, F.-X. Coudert and A. H. Fuchs, *Phys. Chem. Chem. Phys.*, 2010, **12**, 8123–8129.
9 M. De Toni, R. Jonchière, P. Pullumbi, F.-X. Coudert and A. H. Fuchs, *ChemPhysChem*, 2012, **13**, 3497–3503.
10 C. Serre, F. Millange, C. Thouvenot, N. M., G. Marsolier, D. Louer and G. Férey, *J. Am. Chem. Soc.*, 2002, **124**, 13519–13526.
11 T. Loiseau, C. Serre, C. Huguenard, G. Fink, F. Taulelle, M. Henry, T. Bataille and G. Férey, *Chem. Eur. J.*, 2004, **10**, 1373–1383.
12 C. Serre, S. Bourrelly, A. Vimont, N. A. Ramsahye, G. Maurin, P. L. Llewellyn, M. Daturi, Y. Filinchuk, O. Leynaud, P. Barnes and G. Ferey, *Adv. Mater.*, 2007, **19**, 2246–2251.
13 Y. Liu, J.-H. Her, A. Dailly, A. J. Ramirez-Cuesta, D. A. Neumann and C. M. Brown, *J. Am. Chem. Soc.*, 2008, **130**, 11813–11818.

14 A. V. Neimark, F.-X. Coudert, C. Triguero, A. Boutin, A. H. Fuchs, I. Beurroies and R. Denoyel, *Langmuir*, 2011, **27**, 4734–4741.

15 S. Bourrelly, B. Moulin, A. Rivera, G. Maurin, S. Devautour-Vinot, C. Serre, T. Devic, P. Horcajada, V. A., G. Clet, M. Daturi, J.-C. Lavalley, S. Loeran-Serna, R. Denoyel, P. L. LLewellyn and G. Férey, *J. Am. Chem. Soc.*, 2010, **132**, 9488–9498.

16 S. Devautour-Vinot, G. Maurin, F. Henn, C. Serre and G. Férey, *Phys. Chem. Chem. Phys.*, 2010, **12**, 12478–12485.

17 P. Hohenberg and W. Kohn, *Phys. Rev.*, 1964, **136**, B864–B871.

18 W. Kohn and L. J. Sham, *Phys. Rev.*, 1965, **140**, A1133–A1138.

19 N. Guillou, F. Millange and R. I. Walton, *Chem. Commun.*, 2011, **47**, 713–715.

20 F. Salles, S. Bourrelly, H. Jobic, T. Devic, V. Guillerm, P. Llewellyn, C. Serre, G. Férey and G. Maurin, *J. Phys. Chem. C*, 2011, **115**, 10764–10776.

21 F. Paesani, *Mol. Simulat.*, 2012, **38**, 631–641.

22 J. Cirera, J. C. Sung, P. B. Howland and F. Paesani, *J. Chem. Phys.*, 2012, **137**, 054704.

23 L. Chen, J. P. S. Mowat, D. Fairen-Jimenez, C. A. Morrison, S. P. Thompson, P. A. Wright and T. Düren, *J. Am. Chem. Soc.*, doi:10.1021/ja403453g.

24 F.-X. Coudert, R. Vuilleumier and A. Boutin, *ChemPhysChem*, 2006, **7**, 2464–2467.

25 F.-X. Coudert, F. Cailliez, R. Vuilleumier, A. H. Fuchs and A. Boutin, *Faraday Discuss.*, 2009, **141**, 377–39.

26 R. Car and M. Parrinello, *Phys. Rev. Lett.*, 1985, **55**, 2471–2474.

27 D. Marx and J. Hutter, Modern Methods and Algorithms of Quantum Chemistry, Forschungszentrum Jülich, NIC Series, 2000, pp. 301–449.

28 H. J. C. Berendsen, J. P. M. Postma, W. F. van Gunsteren, A. DiNola and J. R. Haak, *J. Chem. Phys.*, 1984, **81**, 3684–3690.

29 N. Troullier and J. L. Martins, *Phys. Rev. B*, 1991, **43**, 1993–2005.

30 J. P. Perdew, K. Burke and M. Ernzerhof, *Phys. Rev. Lett.*, 1996, **77**, 3865–3868.

31 S. Grimme, *J. Comp. Chem.*, 2006, **27**, 1787–1799.

32 A. K. Soper, *Chem. Phys.*, 2000, **258**, 121–137.